NANO LETTERS

LETTER

pubs.acs.org/NanoLett

Softened Elastic Response and Unzipping in Chemical Vapor Deposition Graphene Membranes

Carlos S. Ruiz-Vargas,[†] Houlong L. Zhuang,[‡] Pinshane Y. Huang,[†] Arend M. van der Zande,[§] Shivank Garg,[∥] Paul L. McEuen,[§,⊥] David A. Muller,[†,⊥] Richard G. Hennig,[‡] and Jiwoong Park*[,∥,⊥]

[†]School of Applied and Engineering Physics, [‡]Department of Material Science and Engineering, [§]Department of Physics, [∥]Department of Chemistry and Chemical Biology, and [⊥]Kavli Institute at Cornell for Nanoscale Science, Cornell University, Ithaca, New York 14853, United States

Supporting Information

ABSTRACT: We use atomic force microscopy to image grain boundaries and ripples in graphene membranes obtained by chemical vapor deposition. Nanoindentation measurements reveal that out-of-plane ripples effectively soften graphene's in-plane stiffness. Furthermore, grain boundaries significantly decrease the breaking strength of these membranes. Molecular dynamics simulations reveal that grain boundaries are especially weakening when subnanometer voids are present in the lattice. Finally, we demonstrate that two graphene membranes brought together form membranes with higher resistance to breaking.

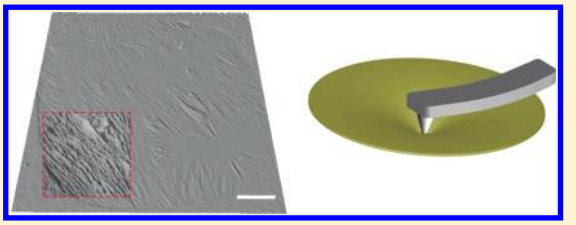

KEYWORDS: Graphene, grain boundaries, AFM, membranes, CVD, molecular dynamics simulations

The excellent mechanical properties of pristine graphene, such as an extremely high in-plane stiffness (Young's modulus) and high breaking strength,[1] along with its unusual electronic properties, make graphene an excellent material for use in applications such as flexible electronics[2] and nanomechanical systems.[3,4] Recent advances using chemical vapor deposition (CVD) have paved the way for the production of single layer graphene on technologically relevant scales. Large-area graphene can be grown on metal surfaces and transferred to a variety of substrates.[5−10] Most notably, graphene growth on copper can be limited to a single layer,[8] enabling novel methods for batch fabrication of graphene devices.[11−13] CVD graphene should be an ideal material for mechanical device applications because in theory, it combines practicality with the excellent mechanical properties of exfoliated graphene.

However, recent work has shown that CVD graphene membranes are composed of multiple grains stitched together by lines of atomic defects.[14] In addition, strains induced during growth and transfer processes cause out-of-plane rippling in free-standing membranes. The understanding of these effects on the mechanical properties of CVD graphene is still limited and is critical to achieving the full potential of graphene in mechanical applications. Here, we use atomic force microscopy (AFM) and nanoindentation measurements and molecular dynamic simulations to study the effect of these unique features on the mechanical properties of CVD graphene.

Our samples were made by transferring CVD graphene, grown on copper foil, onto silicon nitride grids with arrays of prepatterned holes (Figure 1a). The transfer was done by spinning a thin PMMA layer onto the copper foil and etching the metal away with a ferric chloride aqueous solution.[8] The resulting membrane is scooped into a series of rinsing water baths and finally transferred to the target substrate. The yield is significantly increased if the PMMA layer is removed by baking the substrates in air avoiding the use of liquid solvents (Supporting Information).[13,14] The graphene sheets adhere well to the supporting surface, which is important for the nanoindentation measurements described later.

First, we characterize the topography and structure of the CVD graphene membranes using AFM. Figure 2a shows the topography of one suspended membrane, which is clamped on all sides. The membrane appears taut at its edges, without the presence of slack or major corrugations. Detailed imaging, however, reveals that the membranes are rippled on the nanometer scale (Figure 2a, inset). The surface roughness of these sheets is ∼3 nm (rms), with ripples measuring a few nanometers in amplitude.

It is likely that the observed ripples in our membranes are the result of a combination of factors inherent in the growth and transfer process. CVD graphene is not flat to begin with, as it is grown on a copper substrate with surface roughness comparable to that of the graphene membranes (3−6 nm, rms, Figure S1 in the Supporting Information).[15] This inherent nonflat topography could then in turn lead to rippling once the membrane is transferred and subjected to the constraints imposed by the edges of the holes in the supporting substrate. Nonuniform adhesion of membrane to the edges of the holes[16] could cause anisotropic pretension and the irregular transfer process could cause shear

Received: February 5, 2011
Revised: April 16, 2011
Published: April 29, 2011

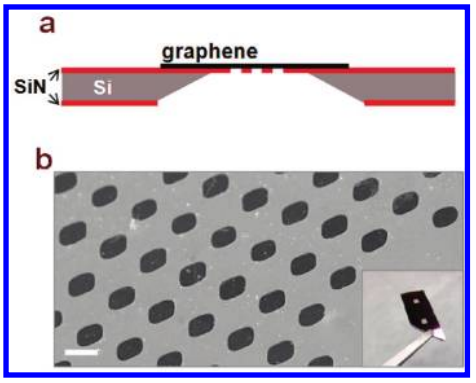

Figure 1. (a) Schematic of substrate with arrays of suspended graphene and (b) SEM image of high yield array of suspended graphene regions. Scale bar: 2 μm. (Inset: optical image of a chip with two holey silicon nitride membranes visible.)

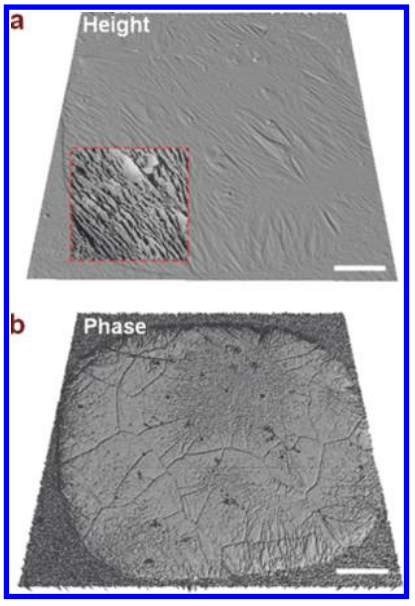

Figure 2. (a) AFM height and (b) phase tapping mode images of a suspended graphene membrane, with grain boundaries clearly visible in the phase image. A region in the image in (a) is shown enlarged in the z direction (height) to accentuate the rippling in graphene. Scale bar: 500 nm.

strain, all of which may result in wrinkling in the membrane. For instance, a shear strain as small as 0.5% would result in ripples with a ratio of amplitude to wavelength comparable to the one we have observed in our membranes.[17,18] Furthermore, thermal cycling has been shown to cause corrugations in graphene and graphene oxide membranes.[19,20] We expect that some inward slipping due to graphene's negative thermal expansion coefficient will further affect the final topography of our membranes without bringing them to a fully relaxed state. Finally, the presence of grain boundaries and defects is predicted to induce topography changes in fully suspended graphene, although perhaps to a lesser extent.[21,22] Further experiments would be required to determine the exact origin of the final topography of our membranes, but such experiments would be difficult with the current membrane fabrication techniques. However, the presence of wrinkles and their effect on the membrane mechanics, described below,

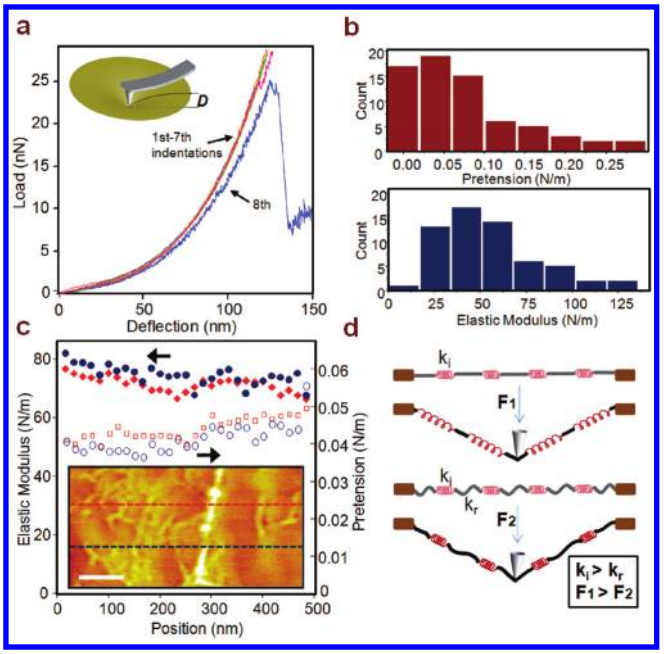

Figure 3. (a) Consecutive indentation measurements taken at the same location of a graphene membrane with side length ~3.5 μm are shown. Inset: schematic of the nanoindentation measurements. (b) Histograms of 2D pretension and 2D effective elastic modulus calculated from similar force curves measured from 60 devices of the same dimensions. (c) Plots of 2D pretension and effective elastic modulus vs position measured from a graphene sheet. They stay nearly constant, even across grain boundaries. Data points were taken along the dashed lines in the AFM phase image shown. Scale bar: 100 nm. (d) Model illustrating a flat and a rippled graphene cross section. The springs have a spring constant k_i representing graphene's intrinsic elastic modulus. However, flattening ripples, which have a much smaller spring constant k_r, requires less energy than stretching the membrane.

highlight some of the general challenges that will be encountered when designing and fabricating devices with free-standing single layer graphene, including the large array mechanical resonators recently reported.[13]

Figure 2b shows a phase image of the same regions as Figure 2a. Strikingly, phase imaging reveals thin lines in the suspended membranes, which are barely visible in height images. By direct correlation with STEM and DF-TEM imaging[14] (see also Figure S5 in the Supporting Information), we identify these features as graphene grain boundaries. STEM and electron energy loss spectroscopy (EELS) characterization of these membranes have identified nanoparticles (mostly iron oxide originating from the $FeCl_3$ based Cu etchant) and amorphous carbon adsorbed at the grain boundaries.[14] These surface adsorbates are likely responsible for the contrast in phase images. These imaging details allow for spatially resolved nanoindentation measurements with respect to the location of the graphene grain boundaries.

We performed a series of nanoindentation measurements to measure the mechanical properties of graphene membranes. Figure 3a shows force−deflection curves obtained by pushing the AFM tip down onto the graphene membrane. From the measured vertical position of the AFM cantilever, and the tip deflection one obtains the distance that the graphene membrane deflects under a given force (Figure 3a, inset). We calculate the membrane's pretension as well as its effective 2D elastic modulus

dx.doi.org/10.1021/nl200429f |*Nano Lett.* 2011, 11, 2259–2263

from these force curves, using the expression

$$F = 2\pi\sigma d/\ln\frac{a}{r} + E(qd)^3/a^2$$

Here, σ and E are the 2D pretension and 2D effective Young's modulus, respectively. The parameters, d, a, and r, are the vertical deflection, the membrane's radius, and the radius of the AFM tip, respectively. Finally, q (which is roughly 1.02)[1] is a function of Poisson's ratio. Our model differs slightly from the one described by Lee. et al.[1] by taking the size of the indenter into account in the linear term of the equation.[16,23] From similar measurements taken on 60 membranes, we find an average effective 2D elastic modulus of 55 N/m with a large fwhm distribution of ~50 N/m (Figure 3b). Our average value is a factor of ~6 smaller than the intrinsic elastic modulus of graphene.[1] We also find an average pretension of 0.085 N/m, in good agreement with the mechanical resonance frequencies found in similarly fabricated devices (Supporting Information).[13] As shown in Figure 3a, reproducible curves are obtained when performing repeated measurements on the same spot. Complete membrane failure is observed in the last force curve in Figure 3a, where a weakened mechanical response is followed by a sudden drop in the force exerted by the tip. Not only are measurements reproducible at the same location, but they also remain approximately constant over a large area. As shown in Figure 3c, the 2D pretension and the effective elastic modulus do not vary significantly when crossing a grain boundary and many graphene ripples. Thus, grain boundaries and ripples do not locally affect the elastic response of the graphene membranes within the limits of our measurements.

We believe that the ripples play a role in the softening of CVD graphene membranes, as previously suggested.[24] To illustrate this, we consider a rippled membrane with negligible bending rigidity. Such a membrane would appear to stretch when subject to an indentation measurement, as its ripples in a given direction flatten out (Figure 3d). In graphene, the bending energy can be neglected for the case of the typical ripples observed on our samples;[25] the force required to flatten out its ripples is considerably less than the force needed to cause in-plan stretching of this membrane. We can approximate a typical height profile across a rippled graphene membrane 3.5 μm in diameter by a sinusoidal function $A\sin(2\pi x/\lambda)$, with amplitude A of ~2 nm and wavelength λ of ~70 nm. If subject to vertical indentation, ripples along this direction would only completely flatten out for vertical deflections d > 200 nm, which is comparable to the maximum deflections we reached in our measurements. Thus, we expect ripple flattening to occur throughout the indentation cycle. The finite effective spring constant of these ripples, and consequently the overall mechanical response of these membranes, will be determined not only by graphene's intrinsic bending modulus but also by the ripple structure and boundary conditions under a given stress field.

As we have previously reported,[14] mechanical failure of CVD graphene typically occurs at the grain boundaries at vertical loads 1 order of magnitude lower than those in exfoliated graphene.[1] To better understand the effect of grain boundaries on graphene's breaking strength, we perform spatially resolved nanoindentation measurements, where the vertical load attained before membrane failure is recorded as a function of tip position. Figure 4a shows a histogram of the breaking loads of 29 graphene membranes, directly on top of grain boundaries and at average distances 300 nm away from a boundary. The average breaking loads, on and away from a grain boundary, are ~50 and

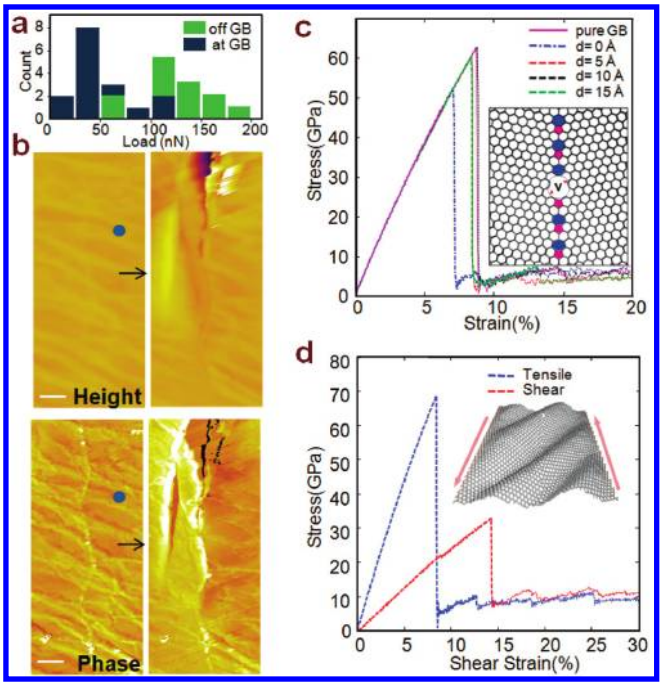

Figure 4. (a) Breaking load histograms for force measurements performed at a grain boundary or away from a grain boundary (on average, 300 nm from a grain boundary). (b) Height and phase AFM images show the region before and after an indentation measurement performed near a grain boundary (at the location indicated by the circle). As seen in the phase image (bottom) graphene tears along a grain boundary. Scale bars: 150 nm. (c) MD simulations of the effect of a void on the strength of a small bicrystalline graphene sheet, varying its position with respect to a grain boundary. Inset: Schematic of model for the simulations for bicrystalline graphene with a void. (d) MD simulation of decreased breaking strength due to shearing in the presence of a grain boundary, as shown in the inset.

~120 nN, respectively. Figure 4b shows images of a region in a graphene membrane with a grain boundary before and after indentation. The weakening effect of grain boundaries can be directly visualized in these AFM images, where tears in the membrane can be seen to follow the direction and path of a grain boundary.[14] Once tearing in a membrane starts, a process analogous to unzipping can occur if this tearing happens at a grain boundary.

From indentation measurements performed at grain boundaries, we estimate the upper bound for the in-plane breaking stress to be ~35 GPa, on the majority of membranes. For this estimate we assume that membrane failure starts directly under the indenter and we use the expression

$$\sigma_{max} = \sqrt{\frac{FE_{int}}{4\pi r}}$$

Here, F is the vertical breaking force, E_{int} is the intrinsic 2D elastic modulus of graphene, and r is the radius of the indenter.[1,26] However, a recent theoretical study predicts the in-plane breaking stress for polycrystalline graphene to be in the range of 50−100 GPa, depending on the type of grain boundary.[27] The discrepancy in the breaking stress in our membranes with these theoretical predictions suggests that grain boundaries alone are not responsible for the small breaking forces in our graphene membranes. Molecular dynamics (MD) simulations on a

dx.doi.org/10.1021/nl200429f |Nano Lett. 2011, 11, 2259–2263

simplified system, undergoing uniaxial strain, shed some light on this issue (Supporting Information).

We considered an alteration to existing theoretical models, including voids into a bicrystalline model, which may further lower the breaking strength closer to the experimentally measured values. Our model membrane is illustrated in Figure 4c, for a graphene grain boundary with misorientation angle of 21.8°. First, the distance between a void and a grain boundary is varied (d = 0, 5, 10, and 15 Å); Figure 4c shows the corresponding stress−strain curves. For comparison, we also plotted the stress−strain curve for a pure grain boundary system. When such a void lies exactly along the grain boundary, the maximum stress is reduced about 15%, while voids near but not on the grain boundary have only a minute effect on graphene's mechanical strength. Additional voids along the grain boundary will further decrease the failure stress of the membrane (Figure S7, Supporting Information), likely increasing the probability that unzipping along a grain boundary will occur. Not surprisingly, the effect of void size is even more pronounced in reducing the strength of bicrystalline graphene (Figure S7, Supporting Information). In short, the possible existence of different voids in graphene could couple with the grain boundaries formed by five to seven member pairs, strongly decreasing CVD graphene's mechanical strength.

However, the loading conditions at the grain boundaries during AFM indentation are not a pure tension problem, since grain boundaries will often be oriented at an angle with respect to the radially directed tension induced by indentation, resulting in shear of the grain boundaries (Supporting Information). We performed additional simulations to consider shearing, which is also present in AFM indentation experiments. The same grain boundary structure is used, applying a pure shear instead of tension, as shown in Figure 4d. Interestingly, the effect of shearing is significant and can cause additional weakening of graphene in the presence of grain boundaries. To further investigate this important role played by shearing loads, we implemented a slightly more complex and realistic model (Figure S8d, Supporting Information), containing four grains with random misorientation angles. We observed that the fracture starts from a boundary lying at an angle with respect to the tensile direction; under the combined effect of shear and tensile loads, this grain boundary tears before others. Thus, grain boundaries appear to be especially vulnerable to complex load conditions which include a shear component. Together, our experimental and theoretical results suggest that an unzipping process at the grain boundaries can occur for loads smaller than those required to break a pristine grain boundary.

Despite its high throughput in fabrication, the reduced breaking strength in CVD graphene can be undesirable for some applications. Here we demonstrate a possible approach to make stronger CVD graphene membranes. We created double layer membranes by simultaneously transferring a PMMA/graphene layer onto both sides of a nitride grid (Figure S3, Supporting Information) and then removing PMMA as previously described. This results in a double layer over the holes in the nitride grid (Figure 5a,b). We measured the resulting membranes and found that the effective 2D elastic modulus measured is roughly doubled compared with results from single layer graphene. We also observed that the strength of the resulting structure increased accordingly. For 13 double-layer graphene samples studied, we found an average breaking force of 230 nN, roughly twice the breaking force of single layer graphene which undergoes indentation away from grain boundaries. One interesting observation in these double layers was the overall mechanical

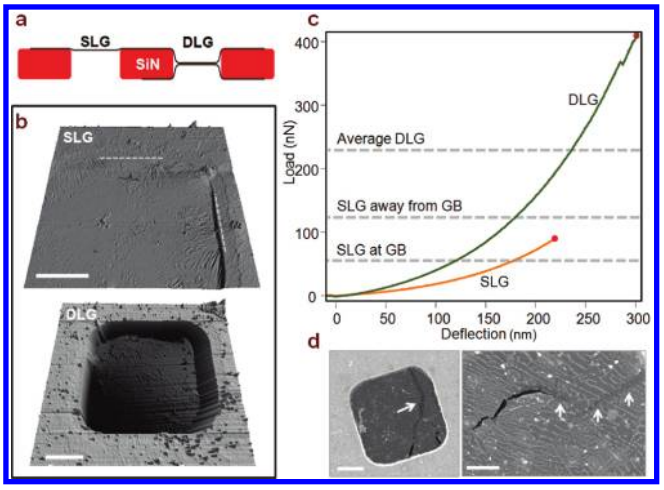

Figure 5. (a) Cross section schematic of single layer graphene (SLG) and double layer graphene (DLG) on a silicon nitride grid. (b) AFM height images of a single layer graphene membrane and a double layer graphene membrane. A single layer graphene membrane lies flatter on the surface of the grid (edge of suspended region indicated by dashed line). Scale bars: 2 μm. (c) Force curves for single and double layer graphene, indicating the increased breaking force resulting from the strengthening addition of a second layer. Average breaking forces for a double layer and single layers are also shown. (d) Scanning electron micrographs of partially broken double layer graphene membrane. The "zebra-like" white lines are caused by residues of the wet transfer process, likely trapped between the two graphene layers. Scale bars: 2 μm (left) and 1 μm (right).

resilience of the membranes during fabrication and indentation measurements. Initial breakages in these double layer membranes, are not immediately followed by complete failure, in contrast to single layer membranes. This can be directly seen when one of the layers starts tearing (Figure 5d), as the other layer will continue to provide structural support for the rest of the membrane (in the scanning electron micrographs, darker shades indicated by the arrows are single layer, and in the black regions both graphene layers are missing). Because of this additional support, the double layer membranes were more likely to survive the fabrication process. This was observed in a significantly increased yield for large suspended bilayer membranes compared to single layer membranes of the same size (Figure S3c, Supporting Information).

While we found that CVD graphene membranes behave differently than those fabricated with exfoliated graphene, our results suggest that controlling the ripple structure, either during the graphene growth or through external shear control, could be used as a knob to change a membrane's out of plane stiffness. Furthermore, improved synthesis techniques for producing graphene membranes with larger grain size[14,28] will prove critical for achieving CVD graphene with high breaking strengths. Novel applications for graphene would greatly benefit from this progress, which can be assessed with these mechanical characterization techniques. CVD graphene membranes could be used, among some examples, as nanomechanical mass sensors, in flexible and transparent electronic devices, or as atomically thin separation windows to isolate different environments.

■ ASSOCIATED CONTENT

Supporting Information. Fabrication procedures as well as additional details on experimental and theoretical aspects. This material is available free of charge via the Internet at http://pubs.acs.org

AUTHOR INFORMATION

Corresponding Author
*E-mail: jpark@cornell.edu.

ACKNOWLEDGMENT

We thank Jonathan Alden for helpful discussions at the initial stages of this project. We also thank Mark Levendorf, Lola Brown, Zenghui Wang, and Chibeom Park for their help during the preparation of the manuscript. This work was supported by the NSF through the Cornell Center for Materials Research and the AFOSR-PECASE award. Sample fabrication was performed at the Cornell Nanoscale Science and Technology Facility, the Cornell node of the National Nanofabrication Infrastructure Network, funded by the NSF. C.S.R.-V. acknowledges support from a Cornell-CONACyT Fellowship, jointly funded by Cornell University and CONACyT-Mexico.

REFERENCES

(1) Lee, C.; Wei, X.; Kysar, J. W.; Hone, J. *Science* **2008**, *321*, 385–388.
(2) Bae, S.; Kim, H.; Lee, Y.; Xu, X.; Park, J.; Zheng, Y.; Balakrishnan, J.; Lei, T.; Ri Kim, H.; Song, Y. I.; Kim, Y.; Kim, K. S.; Ozyilmaz, B.; Ahn, J.; Hong, B. H.; Iijima, S. *Nat. Nanotechnol.* **2010**, *5*, 574–578.
(3) Bunch, J. S.; v.d. Zande, A.; Verbridge, S. S.; Frank, I. W.; Tanenbaum, D. M.; Parpia, J. M.; Craighead, H. G.; McEuen, P. L. *Science* **2007**, *315*, 490–493.
(4) Chen, C.; Rosenblatt, S.; Bolotin, K. I.; Kalb, W.; Kim, P.; Kymissis, I.; Stormer, H. L.; Heinz, T. F.; Hone, J. *Nat. Nanotechnol.* **2009**, *4*, 861–867.
(5) Yu, Q.; Lian, J.; Siriponglert, S.; Li, H.; Chen, Y. P.; Pei, S. *Appl. Phys. Lett.* **2008**, *93*, 113103.
(6) Reina, A.; Jia, X.; Ho, J.; Nezich, D.; Son, H.; Bulovic, V.; Dresselhaus, M. S.; Kong, J. *Nano Lett.* **2009**, *9* (1), 30–35.
(7) Kim, K. S.; Zhao, Y.; Jang, H.; Lee, S. Y.; Kim, J. M.; Kim, K. S.; Ahn, J.; Kim, P.; Choi, J.; Hong, B. H. *Nature* **2009**, *457*, 706–710.
(8) Li, X.; Cai, W.; An, J.; Kim, S.; Nah, J.; Yang, D.; Piner, R.; Velamakanni, A.; Jung, I.; Tutuc, E.; Banerjee, S. K.; Colombo, L.; Ruoff, R. S. *Science* **2009**, *324*, 1312–1314.
(9) Lee, Y.; Bae, S.; Jang, H.; Jang, S.; Zhu, S.; Sim, S. H.; Song, Y. I.; Hong, B. H.; Ahn, J. *Nano Lett.* **2010**, *10* (2), 490–493.
(10) Cao, H.; Yu, Q.; Jauregui, L. A.; Tian, J.; Wu, W.; Liu, Z.; Jalilian, R.; Benjamin, D. K.; Jiang, Z.; Bao, J.; Pei, S. S.; Chen, Y. P. *Appl. Phys. Lett.* **2010**, *96*, 122106.
(11) Levendorf, M. P.; Ruiz-Vargas, C.; Garg, S.; Park, J. *Nano Lett* **2009**, *9* (12), 4479–4483.
(12) Aleman, B.; Regan, W.; Aloni, S.; Altoe, V.; Alem, N.; Girit, C.; Geng, B.; Maserati, L.; Crommie, M.; Wang, F.; Zettl, A. *ACS Nano* **2010**, *4* (8), 4762–4768.
(13) van der Zande, A.; Barton, R. A.; Alden, J. S.; Ruiz-Vargas, C.; Whitney, W. S.; Pham, P. H. Q.; Park, J.; Parpia, J. M.; Craighead, H. G.; McEuen, P. L. *Nano Lett.* **2010**, *10* (12), 4869–4873.
(14) Huang, P. Y.; Ruiz-Vargas, C.; v.d. Zande, A.; Whitney, W. S.; Levendorf, M. P.; Kevek, J. W.; Garg, S.; Alden, J. S.; Hustedt, C. J.; Zhu, Y.; Park, J.; McEuen, P. L.; Muller, D. A. *Nature* **2011**, *469*, 389–392.
(15) Rasool, H. I.; Song, E. B.; Allen, M. J.; Wassei, J. K.; Kaner, R. B.; Wang, K. L.; Weiller, B. H.; Gimzewski, J. K. *Nano Lett.* **2011**, *11* (1), 251–256.
(16) Bunch, J. S.; Verbridge, S. S.; Alden, J. S.; van der Zande, A.; Parpia, J. M.; Craighead, H. G.; McEuen, P. L. *Nano Lett.* **2008**, *8* (8), 2458–2462.
(17) The shear, γ, can be estimated with the relation $A\pi/\lambda = (2\gamma - 2\nu\gamma)^{1/2}$, where ν is Poisson's ratio, taken to be 0.165. from graphite's properties.
(18) Wong, Y.; Pellegrino, S. *J. Mech. Mater. Struct.* **2006**, *1*, 27–61.
(19) Robinson, J. T.; Zalalutdinov, M.; Baldwin, J. W.; Snow, E. S.; Wei, Z.; Sheehan, P.; Houston, B. H. *Nano Lett.* **2008**, *8* (10), 3441–3445.
(20) Bao, W.; Miao, F.; Chen, Z.; Zhang, H.; Jang, W.; Dames, C.; Lau, C. N. *Nat. Nanotechnol.* **2009**, *4*, 562–566.
(21) Liu, Y.; Yakobson, B. I. *Nano Lett.* **2010**, *10* (6), 2178–2183.
(22) Yakobson, B. I.; Ding, F. *ACS Nano* **2011**, *5* (3), 1569–1574.
(23) Wan, K.; Guo, S.; Dillard, D. A. *Thin Solid Films* **2003**, *425*, 150–162.
(24) Min, K.; Aluru, N. R. *Appl. Phys. Lett.* **2011**, *98*, 013113.
(25) Shenoy, V. B.; Reddy, C. D.; Ramasubramaniam, A.; Zhang, Y. W. *Phys. Rev. Lett.* **2008**, *101*, 245501.
(26) Bhatia, N. M.; Nachbar, W. *Int. J. Non-Linear Mech.* **1968**, *3*, 307–324.
(27) Grantab, R.; Shenoy, V. B.; Ruoff, R. S. *Science* **2010**, *330*, 946–948.
(28) Li, X.; Magnuson, C. W.; Venugopal, A.; An, J.; Suk, J. W.; Han, B.; Borysiak, M.; Cai, W.; Velamakanni, A.; Zhu, Y.; Fu, L.; Vogel, E. M.; Voelkl, E.; Colombo, L.; Ruoff, R. S. *Nano Lett.* **2010**, *10* (11), 4328–4334.